

Atmospheric pressure chemical vapor deposition of transparent conducting films of fluorine doped zinc oxide and their application to amorphous silicon solar cells

Haifan Liang · Roy G. Gordon

Received: 3 August 2006 / Accepted: 10 November 2006 / Published online: 25 April 2007
Springer Science+Business Media, LLC 2007

Abstract Transparent conducting ZnO:F was deposited using the textured ZnO:F films as the front as thin films on soda lime glass substrates by atmospheric electrode. The short circuit current was increased over pressure chemical vapor deposition (CVD) deposition at similar cells made with fluorine doped tin oxide, but the substrate temperatures of 480–500 °C. The precursors di-ethylzinc, tetramethylethylenediamine and benzoyl fluoride were dissolved in xylene. The solution was nebulized ultrasonically and then flash vaporized by a carrier gas of nitrogen preheated to 150 °C. Ethanol was vaporized separately, and these vapors were then mixed to form a homogeneous vapor mixture. Good reproducibility was achieved using this new CVD method. Uniform thicknesses were obtained by moving the heated glass substrates through the deposition zone. The best electrical and optical properties were obtained when the precursor solution was aged for more than a week before use. The films were polycrystalline and highly oriented with the c-axis perpendicular to the substrate. The electrical resistivity of the films was as low as 50 mΩ/cm. The mobility was about 45 cm²/Vs. The electron concentration was up to 3 × 10²⁰/cm³. The optical absorption of the films was about 3.4% at a sheet resistance of 7 Ω/square. The diffuse transmittance was about 10% at a thickness of 650 nm. Amorphous silicon solar cells were

Introduction
Zinc oxide is a large band gap semiconductor (3.3 eV) with a hexagonal wurzite structure. As a thin film, zinc oxide has many practical applications, such as in solar cells, liquid crystal flat panel displays, energy efficient windows, gas sensors, surface acoustic wave devices, piezoelectric devices, ultrasonic transducers, etc.

Transparent conductors are materials with low electrical resistivity and high transmittance of visible light. Large band gap semiconducting metal oxides such as indium oxide, cadmium oxide, tin oxide and zinc oxide can be doped with impurity atoms to reduce their resistivity while retaining high transparency in the visible spectrum. Zinc oxide has several advantages over the other transparent conducting oxides. Cadmium in all its compounds is toxic and carcinogenic, and organotin precursors are toxic, while zinc compounds are generally non-toxic. Zinc metal is less expensive than tin, indium or cadmium. For solar cell applications, fluorine doped tin oxide currently is the most widely used front electrode, but tin oxide can be reduced in the hydrogen plasma during the silicon deposition process. This results in elemental tin at the silicon interface that can cause optical loss or diffusion, which can lead to degradation in solar cell efficiency. Zinc oxide is more stable

H. Liang
Division of Engineering and Applied Sciences,
Harvard University, Cambridge, USA

Present Address:
H. Liang (✉)
4253 Sora Terrace, Fremont, CA 94555, USA
e-mail: haifan99@netscape.net

R. G. Gordon
Department of Chemistry and Chemical Biology, Harvard
University, 12 Oxford Street, Cambridge, MA 02138, USA

than tin oxide in a plasma reducing environment. Zinc has a much higher optical transmittance than the other transparent conducting oxides. This suggests zinc oxide is much less reactive to oxygen and moisture, and is not spontaneously flammable. The new CVD process based on the chelated precursor is more controllable and reproducible, and may lead to higher solar cell efficiency than tin oxide. For the chelated precursor is more controllable and reproducible, applications in making patterns for liquid crystal display panels, and the films are more uniform. Zn(TMEDA) is a solid that is easily dissolved in organic solvents such as aqueous acids such as dilute hydrochloric acid. These advantages suggest that zinc oxide should be a technically important material for transparent conducting applications.

Zinc oxide films have been successfully deposited by chemical vapor deposition (CVD) [14], sputtering [18], vacuum evaporation [9], spray pyrolysis [22] and other thin film deposition techniques. CVD generally has faster growth rates and better uniformity than the other deposition processes. It is more suitable for large-scale commercial applications. Conductive zinc oxide films have been made by adding impurity dopants such as boron, aluminum, gallium, and indium [23, 24, 25, 31, 32, 34, 35, 36].

In this paper, we report the atmospheric pressure chemical vapor deposition of ZnO:F films using the tetramethylethylenediamine adduct of diethylzinc, $(\text{C}_2\text{H}_5)_2\text{Zn}(\text{CH}_3)_2\text{NCH}_2\text{CH}_2\text{N}(\text{CH}_3)_2$, as the zinc source, benzoyl fluoride ($\text{C}_6\text{H}_5\text{COF}$) as the fluorine dopant, and ethanol ($\text{C}_2\text{H}_5\text{OH}$) as the oxygen source. We also investigated the structural, electrical and optical properties of the films, and their applicability to amorphous silicon solar cells.

Experimental

Precursors

The commonly used zinc precursors for chemical vapor deposition of zinc oxide include diethylzinc ($(\text{C}_2\text{H}_5)_2\text{Zn}$), dimethylzinc ($(\text{CH}_3)_2\text{Zn}$), and zinc acetylacetonate ($(\text{Zn}(\text{C}_5\text{H}_7\text{O}_2)_2)$). Both dimethylzinc and diethylzinc are difficult to handle because they burn spontaneously in air (pyrophoric). They are very reactive to oxygen and moisture, making a CVD process subject to disruption by leaks of air. The resulting films are frequently irreproducible and not uniform. Zinc acetylacetonate is a solid and has low solubility in the common solvents. It is difficult to vaporize as a precursor. Films made with zinc acetylacetonate also have relatively low growth rate and high resistivity ($>10^3 \text{ } \Omega\text{cm}$).

The tetramethylethylenediamine adduct of diethylzinc ($(\text{Et}_2\text{Zn}(\text{TMEDA}))$) was synthesized by reacting diethylzinc with tetramethylethylenediamine. It is a compound with a chelate amine ligand attached to the diethylzinc. The zinc atom of the chelated precursor molecule is less accessible from the solution.

Experimental procedure

The ZnO films were deposited in a belt furnace made by BTU International. The experimental set up is schematically shown in Fig. 1. The substrate temperature was varied from 450 C to 525 C. The injector included a cylindrical shower head with small holes along the side, housed in a cylindrical chamber leading down to a slot 6 mm wide and 124 mm long. It was designed to make uniform films with all the precursors premixed before entering the injector. $\text{Et}_2\text{Zn}(\text{TMEDA})$ was synthesized by reacting diethylzinc in xylene with tetramethylethylenediamine. Benzoyl fluoride (from Alfa AESAR) was mixed with $\text{Et}_2\text{Zn}(\text{TMEDA})$ dissolved in equal weight of xylene.

The most stable containers for precursor storage were fluorocarbon containers (such as Teflon). Glass or polyethylene containers reacted with the precursor and producing residues. Even in the poly-fluorocarbon lined containers there were gradual chemical changes within the solution, leading to CVD results that depended on the time elapsed since the mixing of the benzoyl fluoride into the solution. uniformly thick film could be deposited. The belt speed varied from 0.5 inch/min to 10 inch/min.

Anhydrous ethanol was obtained from Pharmco. The water content in commercial anhydrous ethanol was determined using the Carl-Fischer titration method to be about 0.04 weight %.

The zinc precursor was pumped from a syringe pump to a SONOTEK ultrasonic nozzle that turned the solution into a fine mist of droplets of about 20–50 micron in diameter with dry air. The substrates were first cleansed with soap and water, then rinsed thoroughly with deionized water, then blown dry with dry air. The substrates were put on a substrate holder

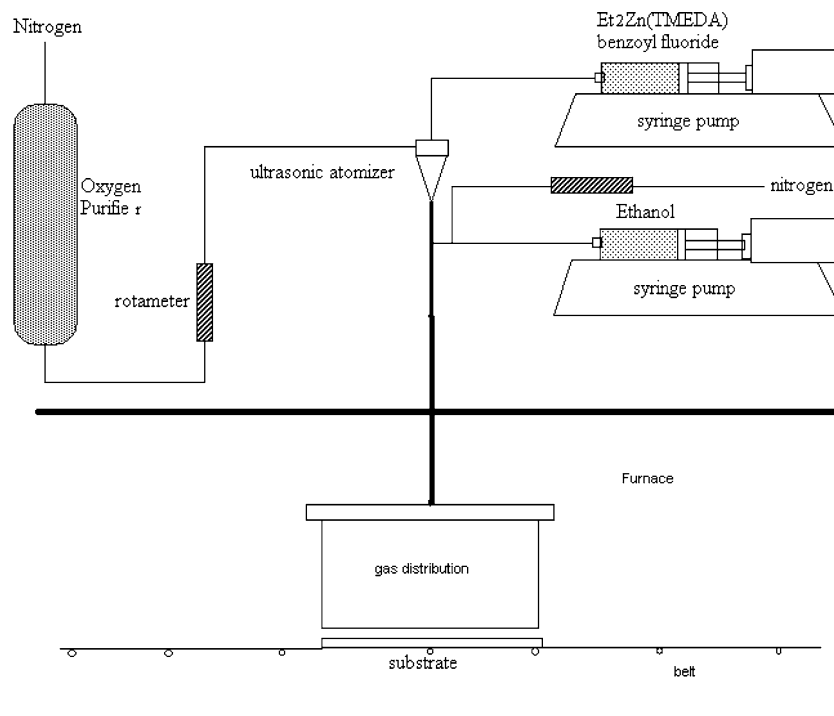


Fig. 1 Schematic drawing of the experimental setup

designed so that the substrate surface was level with the glass substrates did initiate reproducible ZnO growth, substrate holder surface. This produced a more uniform probably by catalyzing the dehydration of ethanol to water. flow across the substrate surface and minimized edges ZnO was grown and covered these oxides, its own effects. The substrate holder was made from either stainless surface also acted as a catalyst for the dehydration of steel or aluminum. The substrate surface temperature was ethanol to grow a next layer of ZnO on top. The results were reproducible when the substrates were precoated with The substrate temperature was 300°C below the furnace any one of these oxides of aluminum, titanium, zinc or tin, temperature. all of which are known to catalyze the dehydration of

Film thickness was measured with a Tencor Alpha-Step 200 profilometer. A step was generated by covering the film with Scotch tape and etching in 4 M HCl. The sheet resistance was measured with a Veeco FPP-100 four point probe. The mobility and electron concentration of the films were measured using van der Pauw's method.

Optical properties were measured with a Hitachi U-4001 spectrophotometer with an integrating sphere detector. For textured ZnO films on glass, light trapped by total internal reflection causes a higher value of the measured absorption. To correct for this effect, an index of refraction of 1.76 was used. Below a substrate temperature of 450°C, very little ZnO was grown. At zinc precursor concentration 0.3 mol%, the film growth rate increased with substrate temperature until 480°C. Above 480°C the growth rate remained the same. At a higher zinc precursor concentration of 0.9 mol%, the growth rate increased with substrate temperature until 510°C. Increasing the precursor concentration required a higher substrate temperature to achieve a similar deposition efficiency. The maximum growth rate was as high as 1,000 nm/min near the entrance of the gas flow. The ethanol concentration did not affect the ZnO growth rate over a broad range. The benzoyl fluoride concentration in the precursor affected the growth rate, and its effect depended on how long the precursor mixture was aged after mixing in the benzoyl fluoride. If the precursor solution was not aged, a high benzoyl fluoride concentration (>3 mol%) strongly inhibited ZnO growth. If the precursor was aged for more than one week, the inhibition effect did not occur until a much higher fluoride concentration was reached. The dependence of the growth rate on fluoride concentration for the aged precursors is shown in Fig. 2.

X-ray diffraction spectra were obtained on a GE X-ray diffraction machine with iron K radiation. The X-ray wavelength was 1.93604 Å. The operating voltage was 40 kV and the current was 10 mA. A manganese filter was used to filter out the iron K α line, but a slight amount of K α radiation still passed through, as could be seen from the small K β line diffraction peaks in the X-ray spectra.

Rutherford backscattering spectra were obtained using a General Ionics Model 4117 spectrometer. The operating He⁺ beam energy was 2.0 MeV. Fluorine concentration was measured using electron microprobe analysis (EMA). It was done on a Cameca MBX electron microprobe using wavelength dispersive spectrometers. The operating beam voltage was 5 keV, beam current was 20 nA, and beam size was 32 μm × 32 μm. The standard for calibration was calcium fluoride.

Film morphology and crystallite size were studied with a LEO 982 Scanning Electron Microscope with GEMINI column.

Results and discussion

Film deposition

Static depositions were first made to study the flow pattern and kinetics of the deposition process. On bare soda lime glass, results were not reproducible and sometimes no film was deposited, or film was only deposited on parts of the substrate. This was attributed to the inability of ethanol to react directly with the zinc precursor. A thin layer (a few tens of nm) of Al₂O₃, TiO₂, ZnO or SnO₂ precoated on the

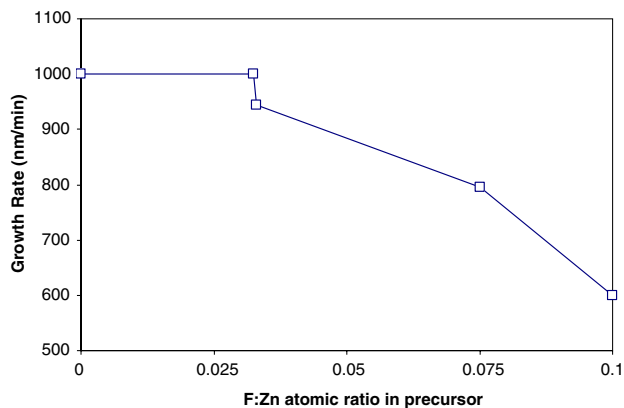


Fig. 2 Dependence of the growth rate on fluorine concentration in the precursor (static deposition, substrate temperature: 495 °C; $\text{Et}_2\text{Zn}(\text{TMEDA})$:0.6 mol%; Ethanol:12 mol%; N_2 :12 l/min)

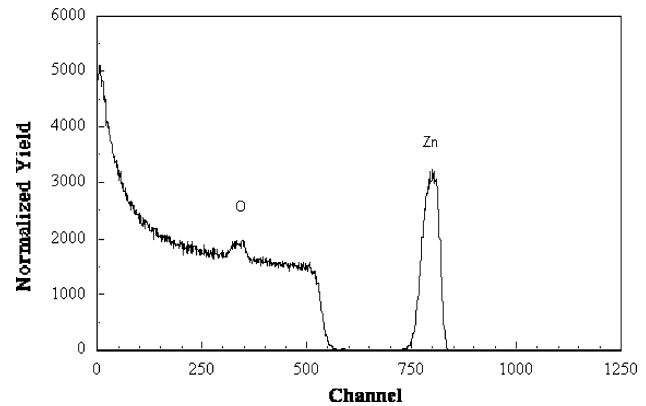


Fig. 3 RBS spectrum of a ZnO:F film (Substrate temperature:495 °C; $\text{Et}_2\text{Zn}(\text{TMEDA})$:0.6 mol%; F/Zn mol ratio:1/27; Ethanol:12 mol%; N_2 :12 l/min; Belt speed:2 inch/min)

uniformly thick films over the entire substrate. It was found that a pre-coating on the soda lime glass substrate was not necessary for uniform film growth during moving depositions. This was attributed to the substrate holder surface next to the substrate, which already had ZnO on top. The ZnO could catalyze the dehydration of ethanol into water and film growth could be initiated on the bare soda lime glass substrate. We confirmed this hypothesis by running depositions on bare soda lime glass substrates without using the substrate holder. The nucleation was poor without the substrate holder, indicating the necessity of an oxide layer to initiate growth. The maximum growth rate for moving deposition was about 240 nm/min.

The deposition efficiency of the reaction for optimal doped films was about 30%.

Composition and crystal structure

Rutherford back scattering (RBS) spectra were obtained for the best electro-optic quality films deposited on silicon. RBS (Fig. 3) spectra showed the zinc oxide films had a Zn:O = 1:1 stoichiometry. No carbon was detected in RBS. Since the fluorine content was very low and the fluorine signal sat on the silicon background, we could not detect the fluorine signal in the RBS spectra. Electron microprobe analysis (EMA) with calcium fluoride as a standard gave fluorine concentration of 0.2–0.3 atomic percent. Since the fluorine concentration was near the detection limit, the results should be taken as only an estimate of the fluorine concentration.

X-ray diffraction patterns of all films grown in this study were crystalline with a hexagonal wurtzite structure. Figures 4 and 5 show the X-ray spectra of undoped and fluorine doped ZnO films grown at 495 °C. Besides a small (103) peak in the undoped film, the main peaks were at $2\theta \approx 32^\circ$ were from iron K β radiation in the X-ray source. The lattice constant of

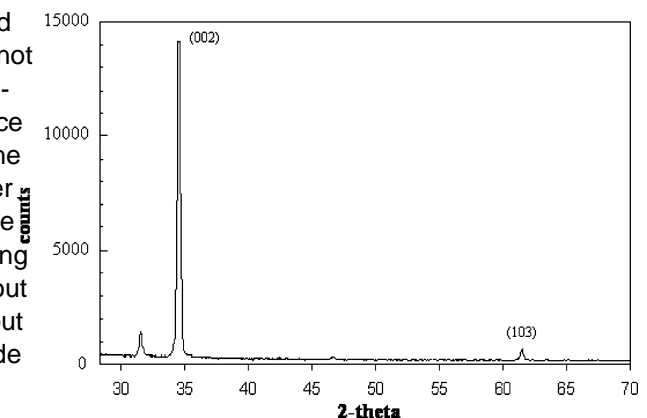


Fig. 4 X-ray spectrum of undoped ZnO (deposition temperature 495 °C), X-ray source: Mn-filtered Fe K lines

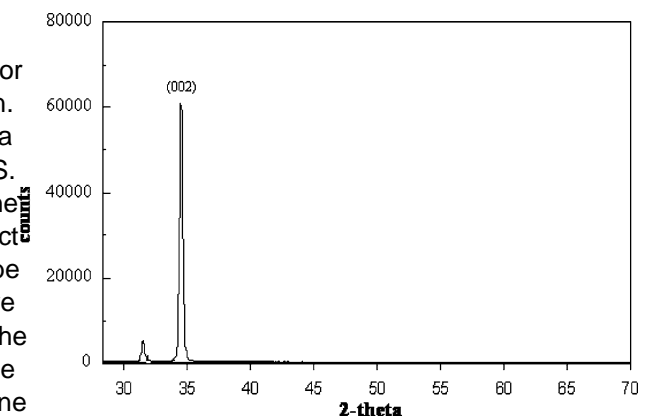


Fig. 5 X-ray spectrum of ZnO:F (deposition temperature 495 °C), X-ray source: Mn-filtered Fe K lines

undoped zinc oxide was $a = 5.193 \text{ \AA}$ closely matching the published value $a = 5.207 \text{ \AA}$ [37]. The fluorine doped PIm had a very slight shift of $D(2\theta) = 0.02$ of the (002) peak towards the lower angles, corresponding to a small increase in the bond length. The n-type doping placed electrons in the anti-bonding conduction band, thereby weakening and lengthening the bonds.

The full width at half maximum of the (002) peaks of both the undoped and fluorine doped ZnO PIm were the same. This indicated the crystallite sizes along the c-axis for both PIm were the same. An estimate of the crystallite size in the direction perpendicular to the substrate was calculated using the Scherrer equation [38]

$$t = 0.9\lambda / \beta \cos\theta \tag{1}$$

where λ is the wavelength of the X-ray, θ is the angular diffraction peak position, and β is the FWHM of the peak. The calculated crystallite thickness was about 30 nm for a PIm 0.8 micron thick.

Electrical properties

Film resistivity was measured from the sheet resistance and the PIm thickness. The PIm deposited using moving substrates had good uniformity in both the PIm thickness and sheet resistance, usually with a variation of less than 10% over the entire substrate area. Variation mainly occurred near the edges. The edge area usually had slightly higher sheet resistance and lower growth rate. This could be due to deposition parameters such as the substrate temperature, dopant concentration, precursor aging time, and ethanol concentration were varied to optimize the PIm resistivity.

The mobility of thin PIm generally increased with the substrate temperature. The optimum substrate temperature was around 480-500 C. At substrate temperatures above 500 C, the mobility and the electron concentration started to decrease. Possible explanations are either the dopant was more difficult to incorporate into the PIm or the dopant was not as electrically active at the higher temperatures. The dependence of the PIm thickness and the electrical properties on substrate temperature is shown in Fig. 6.

The aging time of the fluorine and zinc precursors affected the PIm resistivity. Benzoyl fluoride was premixed with $\text{Et}_2\text{Zn}(\text{TMEDA})$ in xylene solution and stored in a glove box for up to 2 months. Films made with the precursor aged for more than 1 week, but less than 5 weeks had PIm resistivity about 30% lower than the PIm made with precursor aged for less than 1 week. This was probably because the fluorine exchanged with the ethyl group and attached to the zinc atom, resulting in more efficient

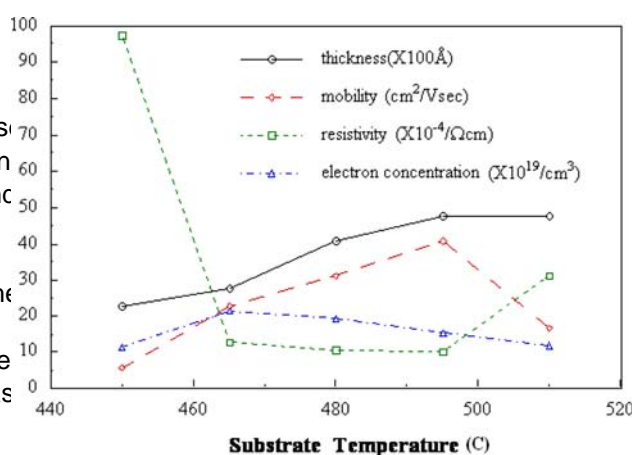


Fig. 6 Electrical properties of ZnO:F PIm as a function of substrate temperature

doping during PIm deposition. However, aging the precursor for more than five weeks resulted in higher PIm resistivity. It was found that both the electron concentration and mobility were lower. This could be due to the formation of zinc fluoride in the precursor or in the PIm. NMR

spectra showed there was a reaction between the zinc and the fluorine precursors over time, but the precise mechanism is not clear.

If the precursor solution was used less than a week after adding the benzoyl fluoride, the PIm resistivity was very sensitive to the precise concentration of fluorine in the precursor. Even a few percent change in the fluorine concentration resulted in large change of the resistivity. The results were difficult to reproduce. For precursor solutions aged more than a week, the resistivity was much less sensitive to the fluorine concentration in the precursor, and the optimum fluorine concentration had a wider range. The

optimum molar ratio of fluorine to zinc was in the range 20 to 1:30. The deposition process was more controllable and reproducible when the precursor was aged for a week or more before use. The dependence of the electrical properties on fluorine concentration in the precursor solution is shown in Figs 7-9.

Ethanol concentration also affected the PIm resistivity. When ethanol concentration was low (below 10:1 ethanol to zinc molar ratio), the PIm had higher resistivity. This

was probably due to carbon contamination in the PIm from the incomplete decomposition of the zinc precursor. The resistivity was optimized over a relatively wide range of ethanol concentration. The optimum molar ratio of zinc to ethanol was about 1 to 20. When the ethanol concentration was too high, the resistivity increased. The increase in resistivity mainly came from a decrease in the carrier concentration, indicating doping was less efficient when the ethanol concentration was high.

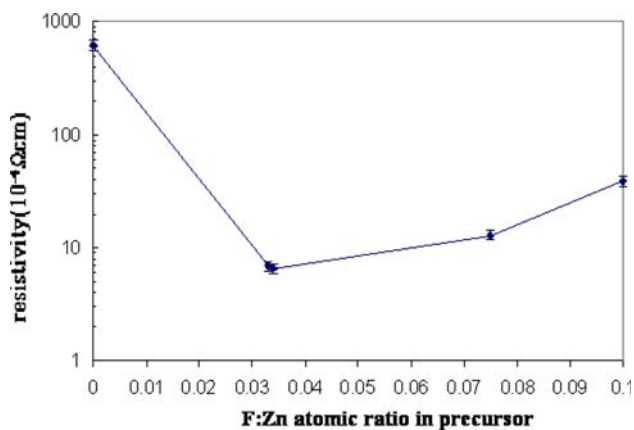


Fig. 7 Dependence of the resistivity of ZnO:F on the fluorine concentration in the precursor

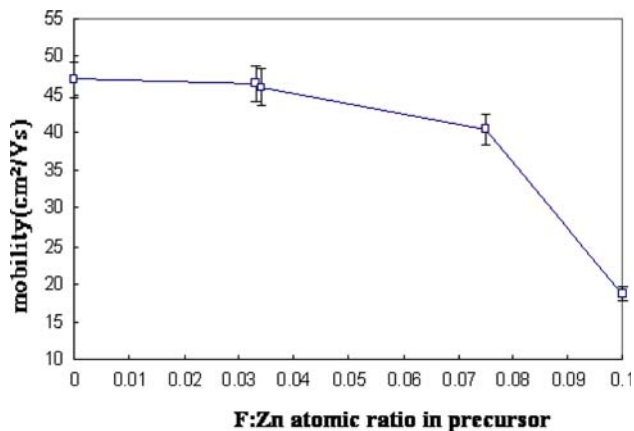


Fig. 8 Dependence of the mobility of ZnO:F on the fluorine concentration in the precursor

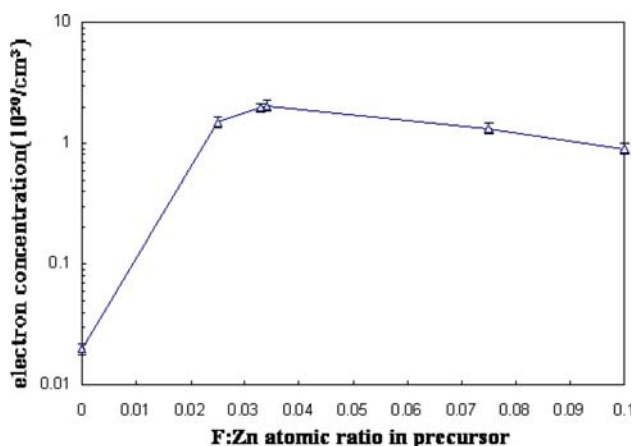


Fig. 9 Dependence of electron concentration of ZnO:F films on the fluorine concentration in the precursor

The resistivity depended on the film thickness. Thinner films had higher resistivity. Generally, the mobility of thinner films was lower because of the smaller grain size. This resulted in larger grain boundary scattering of the free electrons. We found that both the mobility and electron concentration were lower for thinner ZnO:F films. The decrease in electron concentration could be attributed to the increase of trapping states at the grain boundaries when the grain sizes were smaller. Figure 10 shows the dependence of the resistivity on film thickness. The thickness of these films was varied by changing the speed at which the substrate moved across the reaction zone. For films with thickness less than 300 nm, film resistivity depended very strongly on the film thickness, since grain boundary scattering was important for thinner films with small crystallite sizes. For films with thickness greater than 300 nm, film resistivity depended only weakly on the film thickness. Grain boundary scattering was less important when the crystallite sizes were large. The mobility of the thicker films was dominated by ionized impurity scattering. For amorphous solar cell applications, we wanted films with low sheet resistance (<10 Ω /square) and a high diffuse transmittance (>10% near 650 nm); both of these qualities required thick films. We concentrated on investigating films with thickness in the range of 700–900 nm.

The electrical properties of undoped and fluorine doped zinc oxide films were measured for comparison. The only difference in deposition condition was the benzoyl fluoride in the precursor. The optimized fluorine to zinc molar ratio in the precursor was 1:27. The substrate temperature was 495 °C. The zinc precursor concentration was 0.6 mol% in the gas phase. The ethanol vapor concentration was 12 mol%. The total carrier gas flow was 12 l/min. The exhaust flow was 24 l/min. The belt speed was 2 inch/min. Both the undoped and doped films had similar mobility of

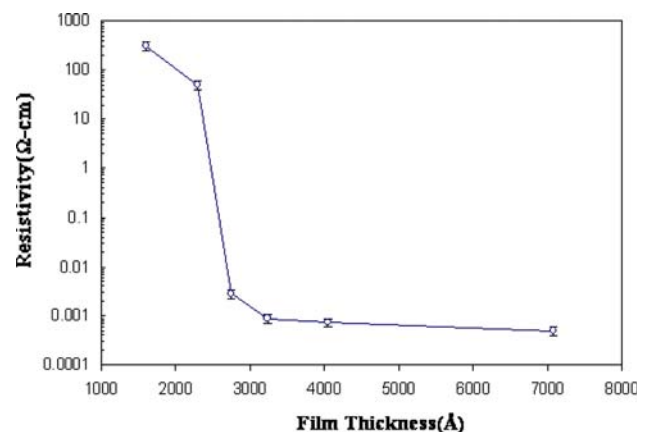


Fig. 10 ZnO:F films resistivity versus thickness (Substrate temperature: 495 °C; Et₂Zn(TMEDA): 0.6 mol%; F/Zn mol ratio: 1/27; Ethanol: 12 mol%; N₂: 12 l/min; Belt speed: 1–10 inch/min)

about 45 cm²/Vs. This was higher than other transparent structure. The crystallites were plate-like and thin in one of the dimensions. The plates were randomly tilted, indicating the crystallites were not completely oriented with the c-axis perpendicular to the substrate surface. Fluorine doped PIm had electron concentration of the order of 10²⁰/cm³, and the fluorine doped PIm had electron concentration of around 10²⁰/cm³. The PIm resistivity of the ZnO:F PIm was as low as 5 · 10⁻⁴ Ωcm.

Fluorine was expected to replace oxygen in the zinc oxide lattice and contribute free electrons, but they also acted as ionized impurity scattering centers. SEM micrographs (Fig.11) showed that when the fluorine concentration in the precursor was high, the grain size decreased.

Grain boundary scattering increased when the grain size decreased. Therefore, the mobility of PIm with high fluorine concentration decreased due to both the increase in ionized impurity scattering and grain boundary scattering. Transmission and reflection spectra were taken to study the optical properties of the PIm. The total transmittance and reflectance of a ZnO PIm with optimum fluorine doping is shown in Fig.12. The PIm thickness was about 800 nm and the sheet resistance was about 17 Ω/square. Optical absorption and texture were the two main optical properties of the PIm. The SEM micrographs (Fig.11) showed the texture is desired to provide light trapping in the cell in order to lengthen the light path in the cell. This is

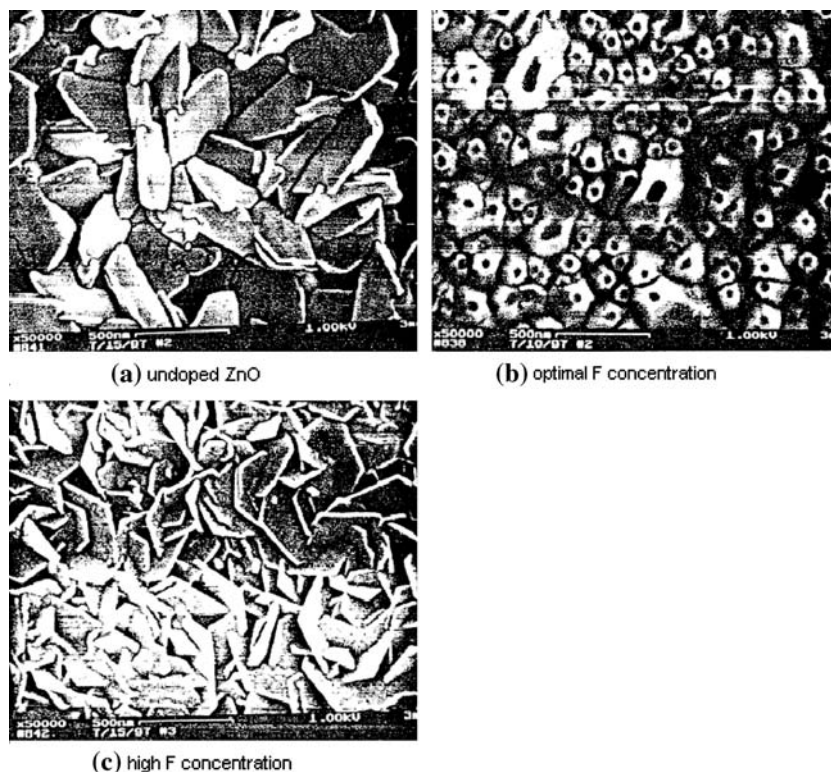


Fig. 11 SEM micrographs of ZnO PIm (a) undoped, (b) optimal F concentration, (c) high F concentration

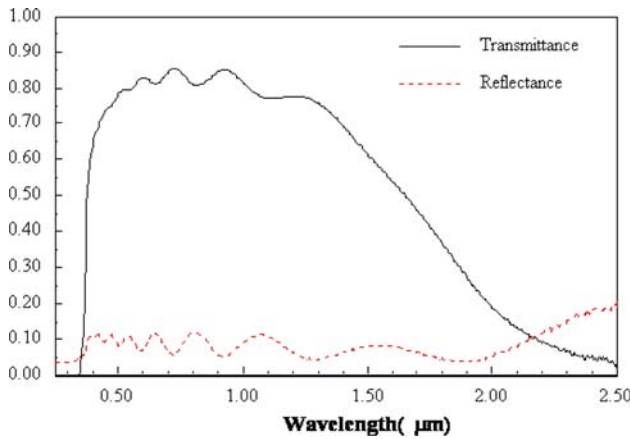


Fig. 12 Total transmittance and reflectance spectra of a ZnO:F film (Sheet resistance: 70 Ω/square, thickness 8,000 angstroms)

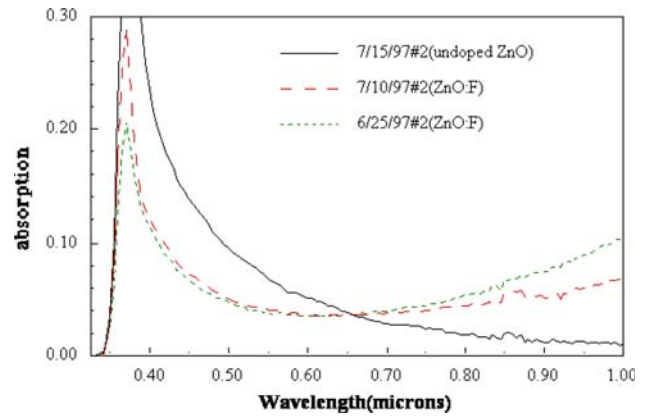


Fig. 13 Optical absorption of undoped and fluorine doped ZnO films (Substrate temperature: 495; Et₂Zn(TMEDA):0.6 mol%; F/Zn mol ratio:0 to 1/27; Ethanol:12 mol%; 2 M l/min; Belt speed:2 inch/min)

especially important for silicon in the near infrared region of the spectrum, since silicon does not absorb strongly in this region.

Deposition conditions such as the substrate temperature, dopant concentration, and ethanol concentration were varied to study the optical absorption of the films. Film absorption was mainly affected by the ethanol concentration. Low ethanol concentration resulted in a brown film with large absorption. This was attributed to carbon contamination due to the incomplete decomposition of the zinc precursor. Optical absorption decreased with increasing ethanol concentration. This had to be compromised with electrical resistivity, since a higher than optimum ethanol concentration increased the film resistivity.

Doping the films with fluorine generated free electrons which modified the optical properties of the films. Increasing the electron concentration in the film also led to increased absorption in the visible region from free electron absorption. The absorption coefficient in the visible region is given by [39]:

$$\alpha = 4\pi k/\lambda = (e^3/4\pi^2 \epsilon_0 c_0^3) \lambda^2 n_e / m^{*2} \mu\text{m} \quad (2)$$

where n and k are the real and imaginary parts of the refractive index, λ is the wavelength, n_e is the free electron concentration, m^* is the effective mass, and μ is the mobility. Since the fluorine doped zinc oxide films had the high mobility and low electron concentration, film absorption was lower than other transparent conductors such as indium tin oxide and fluorine doped tin oxide. The solar weighted average absorption in the wavelength region 400-700 nm was as low as 3-4% for films with a sheet resistance about 70 Ω/square.

Figure 13 shows the absorption spectra of undoped and doped zinc oxide films. The doped zinc oxide film showed increased absorption in the near infrared region due to the

increase in free electron concentration. The doped zinc oxide films had lower absorption in the near ultra-violet region because of the Moss-Burstein effect. The Moss-Burstein effect is partly offset by a band gap narrowing effect due to carrier-carrier interactions and carrier-impurity interactions. For heavily doped films such as the ZnO:F, the Moss-Burstein effect is dominant and the absorption edge shifted to the lower wavelengths. This effect is advantageous in solar cell applications to allow more photons in the near ultra-violet region to enter the cell. It can also be useful in some optoelectronic devices where band gap tailoring is required.

Film texture was measured by the diffuse transmittance of the films. For effective light trapping, about 5% diffuse transmittance at 650 nm is adequate to enhance cell performance [40]. We found that the film texture depended on the substrate temperature, ethanol concentration, and dopant level. Texture increased with the substrate temperature. This was due to the increase in grain size at the higher temperatures. Texture decreased when the ethanol concentration was high. The nucleation density was probably higher when the ethanol concentration was high, leading to smaller crystallite sizes and smoother films. Texture also decreased with increasing fluorine dopant concentration. Figure 14 shows the diffuse transmittance spectra of undoped, optimally doped and highly doped films. For the optimal doped films, more than 10% diffuse transmittance was achieved at 650 nm.

The electrical and optical properties ZnO:F films were stable at room temperature. The thermal stability of the films was studied by annealing the films at 400-500 °C in the furnace for half an hour (Table 1). The furnace was

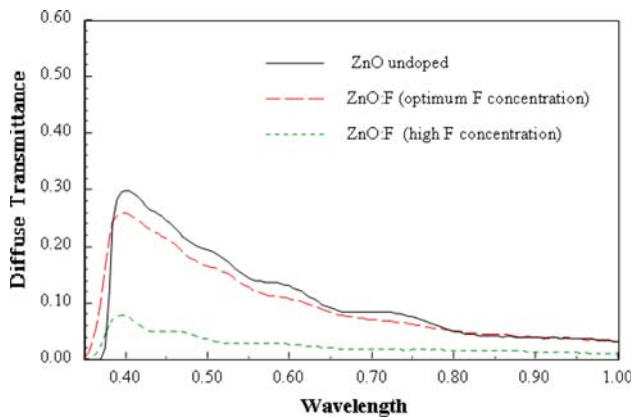


Fig. 14 Diffuse transmittance spectra of undoped and F doped ZnO films (Substrate temperature: 495; Et₂Zn(TMEDA):0.6 mol%; F/Zn mol ratio:0 to 1/9; Ethanol:12 mol%; μ :12 l/min; Belt speed:2 inch/min)

less fluorine and more oxygen vacancies. Their resistivity increased more rapidly when the oxygen vacancies were filled by the ambient oxygen during annealing.

Films were also annealed in 10% oxygen and 90% nitrogen at 400 C to study their stability in an oxygen environment. These films were annealed for about 10 min to simulate the deposition of another layer on the film. The resistivity did not change for films with resistivity less than $8 \cdot 10^{14} \Omega\text{cm}$. The resistivity increased for films with higher resistivity. The percent increase in resistivity was higher when the film resistivity was higher.

Application to amorphous silicon solar cells

The applicability of ZnO:F as a front electrode on a-Si cells were tested at Solarex and University of Delaware. The structure of the cells is shown in Fig. 15. Both groups

filled with large flows of nitrogen, but oxygen could not be reported an increase of about 5% in the short circuit current complete eliminated due to the open construction of using ZnO:F compared to the standard SnO₂ films. This the furnace. At 400C, the resistivity was relatively is consistent with the higher transparency of the ZnO than unchanged after annealing. At higher temperatures, the SnO₂. The open circuit voltages of the cells made on resistivity increased after annealing. The percent increase ZnO:F were, from 10 mV to 100 mV lower than control in resistivity was higher at the higher annealing temperatures. At 500 C, the resistivity was increased by at least a function of ZnO compared to SnO₂ cells on SnO₂. This can be explained by the lower work order of magnitude. Some of the free electrons in the film ZnO:F cells were also lower, by 30-10%, than cells made on could be contributed by oxygen vacancies. Annealing in a SnO₂:F. This is attributed to the higher contact resistivity oxygen containing environment caused oxygen to enter the ZnO/Si than SnO₂/Si. Both the lower work function and film and filled some of the oxygen vacancies. This could the lower electron concentration contributed to the increase reduce the carrier concentration and increase the resistivity in contact resistivity when using ZnO:F. At high annealing temperatures, oxidation was more efficient and there could be sodium diffusion from the soda of ZnO, a thin layer (a few hundred angstroms) of heavily lime glass substrate. Sodium in the film could increase doped SnO₂ was deposited between the ZnO and the p-type defect scattering and lower the mobility. This could also a-Si layer. The SnO₂ layer should be thin enough to retain increase the resistivity. The increase in resistivity was high light transmission, but thick enough to provide good higher for more resistive films. Films with lower resistivity electrical contact. The structure SnO₂/thick ZnO:F/glass should combine the best features of the two materials for the oxygen sites. Therefore there were fewer oxygen a-Si solar cells. The thick ZnO:F should provide high vacancies in the more conductive films and they were more transparency, and the thin SnO₂ should provide good stable under annealing. Films with higher resistivity had electrical contact to the silicon.

Table 1 Sheet resistance change of ZnO:F films annealed in one atmosphere of nitrogen gas for 30 min at various temperatures

| F:ZnO Film | Original sheet resistance (Ω / square) | Sheet resistance after annealing for 30 min | | | | |
|-------------------|--|--|-------|-------|-------|-------|
| | | 400 C | 425 C | 450 C | 475 C | 500 C |
| Sample 10.1 #1 | 10.1 | 12.0 | 13.9 | 29.4 | 527 | |
| Sample 12.9 #2 | 13.6 | 18.9 | 21.7 | 51.0 | 1,900 | |
| Sample 13.6 #3 | 14.6 | 22.4 | 27.8 | 76.4 | 6,600 | |

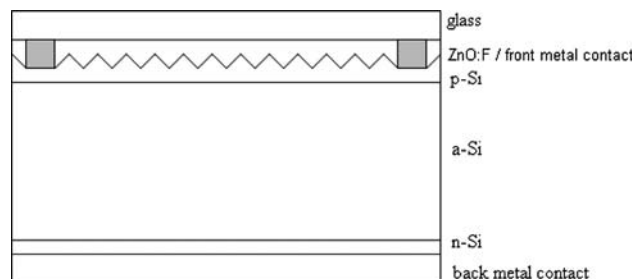


Fig. 15 Structure of an amorphous silicon solar cell with textured ZnO:F front electrode

The standard CVD deposition temperature of SnO₂ above 500 C. This would lead to an increase of sheet resistance in the underlying ZnO:F flm. We investigated the deposition of SnO₂:F at lower temperature, and found SnO₂:F could be deposited at 460 C by the reaction of tetramethyltin, oxygen and hexafluoropropene. The free electron concentration in the SnO₂ was 5 · 10¹⁹ cm⁻³, an order of magnitude lower than the values usually found for optimized SnO₂:F deposited at higher temperatures.

Amorphous silicon solar cells were deposited on samples of the thin SnO₂:F/thick ZnO:F/glass transparent conductors using three different boron dopant levels in the p-Si layer. The lowest β₀ is typical of was used for standard SnO₂ substrates. Figure 16 shows that the standard boron doping level gave lower open-circuit voltages on the ZnO substrate than on SnO₂. The thin, lightly doped SnO₂ layer on the composite SnO₂:F/ZnO:F raised the voltage back to the level found in the same run for standard SnO₂. This result supports the potential of the composite SnO₂:F/ZnO:F to increase cell efficiency.

At the higher levels of boron doping, the voltages became equivalent for all of the substrates. The FF factors increased with boron doping level, but, unfortunately, remained lower for both ZnO-containing substrates, at all boron doping levels (Fig 17). Apparently, a higher free electron concentration will be needed in the tin oxide contact layer, if higher FF factors and efficiencies are to be attained with the composite SnO₂:F/ZnO:F transparent conductor.

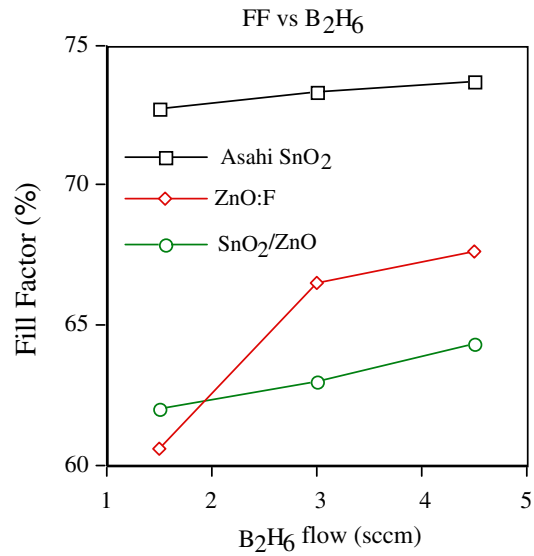


Fig. 17 Fill factors for amorphous silicon solar cells grown on three different transparent conductors, as a function of the boron doping level in the p-layer

Summary

We successfully deposited highly transparent conducting textured ZnO:F flms from Zn(TMEDA), ethanol, and benzoyl fluoride. The new precursor and injector design produced uniform flms with good reproducibility. A catalytic oxide was needed to dehydrate the ethanol and start flm growth on bare glass substrates. The flm growth rate increased with precursor concentration, but the deposition efficiency became lower. The growth rate decreased with fluorine dopant concentration. The flms were polycrystalline and highly oriented with the c-axis perpendicular to the substrate. The crystallites were pointed columnar with diameters between 100 nm and 500 nm and height of about 28 nm. The resistivity decreased with the flm thickness. The aging time of the zinc and fluorine precursor solution affected the electrical and optical properties of the flms. The mobility decreased with dopant concentration and was optimized at about 480-500 C. The mobility was about 45 cm²/Vs. The electron concentration increased with dopant concentration and decreased after a maximum was reached. The electron concentration was up to 10²⁰/cm³. The resistivity was as low as 5 · 10⁻⁴ Ωcm. Film absorption decreased with increasing ethanol concentration, but the conductivity and the texture of the flms decreased when the ethanol concentration was too high. The optimum zinc to ethanol molar ratio was about 1:20. Visible absorption was only 3-4% at a sheet resistance of 7 Ω/square. The diffuse transmittance can be varied from about 1-10% at 6,500 Å. We conclude the excellent electrical and optical properties of the ZnO:F flms, together with

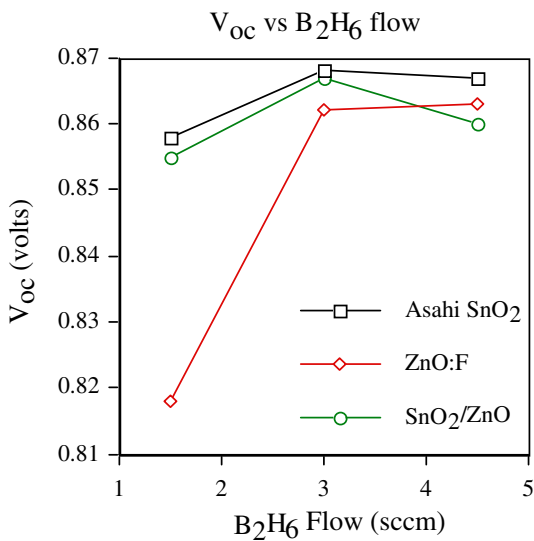


Fig. 16 Open circuit voltages for amorphous silicon solar cells grown on three different transparent conductors, as a function of the boron doping level in the p-layer

good uniformity and reproducibility, makes it an attractive candidate for many applications as a transparent conductor. Application to more efficient amorphous silicon solar cells will require a thin contact layer of highly doped tin oxide.

Acknowledgements This work was supported by the National Renewable Energy Laboratory. Steven Hegedus (Delaware) and David Carlson (Solarex) deposited and characterized the amorphous silicon solar cells. John Thornton, Keith Kramer, Dan Teff and Nicholas DiCeglie provided assistance in the chemical preparations and analyses. The authors would also like to thank Yuan Z. Lu, David Lange, and John Chervinsky for their assistance in making some of the characterization measurements.

References

- Hickernell FS (1976) *Proc IEEE* 64:631
- Dutta S, Jackson HE, Boyd JT, Hickernell FS, Davis RL (1981) *Appl Phys Lett* 39:206
- Igasaki Y, Saito H (1991) *J Appl Phys* 70:3613
- Adachi K, Sato K, Gotoh Y, Nishimura H (1991) *Proc of 22nd IEEE PVSC*
- Adachi K, Sato K, Gotoh Y, Nishimura H (1991) *Proc of 22nd IEEE PVSC*
- Shiosaki T, Yamamoto T, Yagi M, Kawabata A (1981) *Appl Phys Lett* 39:399
- Shiosaki T (1978) *Proc IEEE Ultrasonics Symp* 100
- Shiosaki T, Ohnishi S, Kawabata A (1979) *J Appl Phys* 50:3113
- Oda S, Tokunaga H, Kitajima N, Hanna J, Shimizu I, Kokado H (1985) *Jap J Appl Phys* 24:1607
- Smith FTJ (1983) *Appl Phys Lett* 43:1108
- Kim JS, Marzouk HA, Reucroft PJ, Harmin CE (1992) *Thin Solid Films* 217:133
- Shimizu M, Katayama T, Shiosaki T, Kawabata A (1990) *J Cryst Growth* 101:171
- Wieldraaijer W, van Balen Blanken J, Kupiers EW (1993) *J Cryst Growth* 126:305
- Souletie P, Bethke S, Wessels BW, Pan H (1988) *J Cryst Growth* 86:248
- Webb JW, Williams DW, Buchanan M (1981) *Appl Phys Lett* 39:640
- Minami T, Nanto H, Takata S (1982) *Appl Phys Lett* 41:958
- Exarhos GJ, Sharma SK (1995) *Thin Solid Films* 270:27
- Jacobsohn E, Shehtman D (1992) *Mat Res Soc Symp Proc* 242:779
- Brody DE, R Singh, Morgan JH, Lesli JD, Moore CJ, and A Dixon (1980) In: *Proceedings of the 12th IEEE Photovoltaic Specialist Conference*. IEEE, New York
- Kruncks M, Mellikov E (1995) *Thin Solid Films* 270:33
- Major S, Banerjee A, Chopra KL (1986) *J Mater Res* 1:300
- Aranovich J, Ortiz A, Bube RH (1979) *J Vac Sci Technol* 16:9
- Hu J, Gordon RG (1991) *Solar Cells* 30:437
- Hu J, Gordon RG (1992) *J Appl Phys* 71:880
- Hu J, Gordon RG (1992) *J Electrochem Soc* 139:2014
- Sato H, Minami T, Miyata T, Ishii M (1994) *Thin Solid Films* 246:65
- Minami T, Sato H, Imamoto H, Takata S (1992) *Jpn J Appl Phys* 31:L257; Minami T, Sato H, Sonohara H, Takata S, Miyata T, Fukuda I (1994) *Thin Solid Films* 253:14
- Jin ZC, Hamberg I, Granqvist CG (1988) *J Appl Phys* 64:5117
- Aktaruzzman AF, Sharma GL, Malhotra LK (1991) *Thin Solid Films* 198:67
- Nishino J, S Ohshio, Kamata K (1992) *J Am Ceram Soc* 75:3469
- Tominaga K, Kataoka M, Ueda T, Chong M, Shintani Y, Mori I (1994) *Thin Solid Films* 253:9
- Hu J, Gordon RG (1992) *J Appl Phys* 72:5381
- Hirata GA, McKittrick J, Cheeks T, Siqueiros JM, Diaz JA, Contreras O, Lopez OA (1996) *Thin Solid Films* 288:29
- Wang R, King LLH, Sleight A (1996) *J Mater Res* 11:1659
- Hu J, Gordon RG (1991) *Mat Res Soc Symp Proc* 283:891
- Olvera ML, Maldonado A, Asomoza R, Konagai M, Asomoza M (1993) *Thin Solid Films* 229:196
- Dana's System of Mineralogy, 7th Ed I 504
- Nuffield EW (1966) *X-ray diffraction methods*. John Wiley & Sons, New York
- Chopra KL, Major S, Pandya DK (1983) *Thin Solid Films* 102:1
- Gordon RG, Proscia J, Ellis FB, Delahoy AE (1989) *Solar Energy Mater* 18:263
- Ahmad Nuruddin, PhD Thesis, University of Illinois, 1997; Ahmad Nuruddin and John Abelson, unpublished results